2007

Short-Time Transient Analysis of Intercalation of an Ion into a Sphere

Sheba Devan

Ralph E. White
University of South Carolina - Columbia, white@cec.sc.edu

Publication Info

Published in *Journal of the Electrochemical Society*, Volume 154, Issue 3, 2007, pages A242-A252.

Devan, S. & White, R.E. (2007). Short-Time Transient Analysis of Intercalation of an Ion into a Sphere. *Journal of the Electrochemical Society*, *154*(3): A242-A252.
Publisher's Version: http://dx.doi.org/10.1149/1.2431321

Journal of The Electrochemical Society, **154** (3) A242-A252 (2007)
0013-4651/2007/154(3)/A242/11/$20.00 © The Electrochemical Society

Short-Time Transient Analysis of Intercalation of an Ion into a Sphere

Sheba Devan* **and Ralph E. White****,z**

Center for Electrochemical Engineering, Department of Chemical Engineering, Swearingen Engineering Center, University of South Carolina, Columbia, South Carolina 29208, USA

A short-time transient analysis is presented for a sinusoidal input potential for a spherical particle. The objective of this work was to extract accurate values of the parameters associated with an intercalation into a spherical particle. These parameters are exchange current density, double-layer capacitance, and diffusion coefficient. The effects of these parameters on the response were examined using a sensitivity analysis, which indicated that optimum frequency values of the input perturbation exist for estimation of these parameters. A procedure is presented to obtain all these parameters using the short-time response. The results show that the short-time analysis is a useful method for estimating rapidly the values of these parameters of a system.
 [DOI: 10.1149/1.2431321]

Manuscript submitted May 12, 2006; revised manuscript received November 14, 2006. Available electronically February 2, 2007.

We present a short-time analysis of the current-density response of an intercalation particle to a sine wave input potential in this paper. This response is dictated by two processes occurring at the interface of the electrolyte and the particle and one in the bulk solid. The interfacial processes include an electrochemical reaction and double-layer charging occurring at the interface between the solid and liquid phases. In the bulk of the intercalation particle, diffusion of the intercalation species occurs. Our analysis is based on the particle model for a porous electrode.[1,2] The particle model is fundamentally simple in terms of formulating the model equations and yet is useful for determining the kinetic and transport parameters. The particle model does not include concentration gradients in the solution phase. The intercalation particle has been the subject of study for many researchers, because understanding the physics of the basic unit, an intercalation particle, complements the analysis of the behavior of a larger system that is an assembly of such units, the porous electrode. Both experimental studies facilitated by microelectrode techniques[3-7] and theoretical studies[1,8,9] have enhanced our knowledge of the porous electrodes. Moreover, extension of an intercalation particle model to a complete lithium-ion cell[2,10] has been identified as a suitable model to represent the battery potential at moderate discharge rates.[11]

The periodic steady-state solution and the complete solution, including the initial transients for the response current density of the intercalation particle, were used to perform transient analysis. The nature of the perturbation signal chosen for this study is a sinusoidal perturbation. Investigating the transient response and the effect of parameters and frequency on the transient response revealed the possibility of estimating the diffusion coefficient with the short time response. Sinusoidal perturbation has been chosen because it is a fundamental waveform that can be used to represent any other waveform using the Fourier series.[12] For example, a step-input perturbation can be represented as a series of various sinusoidal waves. Hence, demonstrating the methodology using sinusoidal signals and short-time data implies that the transient technique can be applied to other kinds of perturbations, such as step, pulse, ramp, etc. The time-domain response for a particle model for an applied-current perturbation has been derived when the current is a constant with respect to time, using Laplace transform technique.[13] Later, Liu developed the time-domain response for the same by employing the integral transformation method for both constant and sinusoidal current perturbations.[14] The author argued that the series solution obtained through integral transformation was easier to derive. In this paper, we derive the series solution for the current as a response for an applied-voltage perturbation using the Laplace transform technique. By combining it with the steady-state solution derived separately, not a series solution, the number of terms in the expression for the current response has been considerably reduced. In order to study the effect of each parameter of interest, the variation of the sensitivity coefficient of the parameter of the system (exchange current density, double-layer capacitance, and solid-state diffusion coefficient) is predicted. This sensitivity analysis was also useful for choosing the appropriate operating frequencies to obtain reliable parameter values for the parameters and hence derive a procedure for parameter estimation. Subsequently, the parameters of the system were estimated for three different cases of diffusion-limited, kinetic-limited, and when both the processes are important. In place of experimental data, synthetic data obtained by adding noise to the model results were used. The parameter values and their confidence intervals indicate that the short-time analysis presented here is a reliable method for estimating parameters. Estimation of kinetic and transport parameters of an intercalation particle has been obtained by many researchers using different methods such as electrochemical impedance spectroscopy (EIS),[15-23] potential intermittent titration technique (PITT), galvanostatic intermittent titration technique (GITT),[24-27] and relaxation techniques.[28,29] The techniques used so far have made use of the long-time solutions, which is in contrast to the use of short-time solutions in this paper.

Analytical Solution

For an intercalation particle (see an illustration of the system in Fig. 1), Fick's law of diffusion governs the solid-phase concentration of lithium ions. The governing equation and the boundary conditions are summarized below

Governing equation
$$\frac{\partial c_p}{\partial t} = \frac{D_s}{r^2}\frac{\partial}{\partial r}\left(r^2\frac{\partial c_p}{\partial r}\right) \quad [1]$$

Boundary condition at $r = 0$
$$-D_s\frac{\partial c_p}{\partial r} = 0 \quad [2]$$

Boundary condition at $r = R_s$
$$-D_s\frac{\partial c_p}{\partial r} = \frac{j_{n,f}}{F} \quad [3]$$

where $j_{n,f}$ is the faradaic current density and is given by the Butler–Volmer equation

$$j_{n,f} = i_0\left[\exp\left(\frac{\alpha_a F}{RT}\eta\right) - \exp\left(\frac{-\alpha_a F}{RT}\eta\right)\right] \quad [4]$$

where $\eta = \phi_1 - \phi_2 - U$ and the open-circuit potential, U, and i_0 is a function of the surface concentration of the particle, c_s. The surface concentration is referred as the state of charge, which is the dimensionless quantity

* Electrochemical Society Student Member.
** Electrochemical Society Fellow.
z E-mail: white@engr.sc.edu

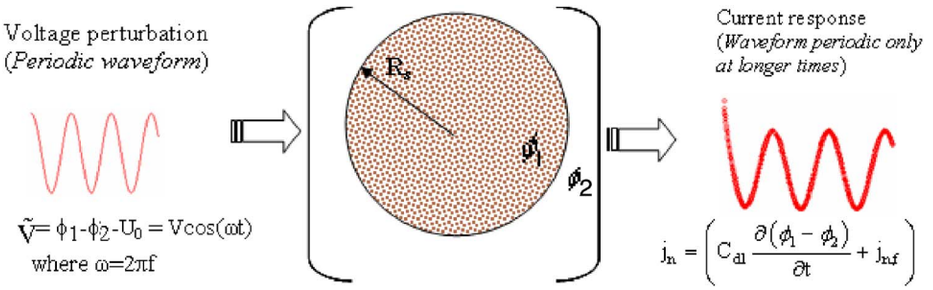

Figure 1. (Color online) Transient analysis of an intercalation particle using a sinusoidal perturbation as the applied voltage.

$$\theta = \frac{c_s}{c_{\max}} \quad [5]$$

The functional form of U and i_0 are[30]

$$U = \frac{1.99 + 2.472\frac{c_s}{c_{\max}}}{1 + 31.823\frac{c_s}{c_{\max}}} \quad [6]$$

and[31]

$$i_0 = k_a(c_{\max} - c_s)^{\alpha_a}(c_s)^{\alpha_c}c^{\alpha_a} \quad [7]$$

where c is the concentration of lithium ions in the solution phase surrounding the particle, which is a constant because it is assumed that the concentration does not change in the solution. The value of c is taken from Ref. 31 and is the initial concentration of lithium ions in the electrolyte. In writing the model equations, other simplifications are made for transient analysis: (*i*) concentration gradients exist only in the solid phase in a spherical particle in the radial direction, (*ii*) the particle is engulfed in an electrolyte media, (*iii*) both double-layer charging and a linear faradic reaction occur at the surface of the particle and they are separable, (*iv*) the charge separated across the double layer is only dependent on the potential difference across the interface, (*v*) the properties (i_0, D_s, α_a, and α_c) are assumed to be constants, (*vi*) the double-layer capacitance (C_{dl}) is a constant, (*vii*) open-circuit potential at the start of the experiment is U_0, and (*viii*) initially, the concentration within the particle is assumed to be uniform and equal to c_p^0 and the corresponding open-circuit potential is U_0, which is a function of c_p^0. The present model is kept simple to limit the number of parameters in the system to investigate the interaction between the processes that occur in a system and their influence on obtaining estimates of the parameters involved. However, the methodology could certainly be extended to other models, taking into account other processes such as the presence of a surface film, resistances, and multiple phases.

When a sinusoidal perturbation of very small amplitude voltage is applied, the current can be linearized with respect to the potential difference between the solid phase and solution phase ($\phi_1 - \phi_2$) and the surface concentration (c_s) as

$$j_{n,f} = \frac{ni_0F}{RT}\left[(\phi_1 - \phi_2 - U_0) + \left(-\frac{\partial U}{\partial c_s}\right)\Big|_{c_s^0,U}(c_s - c_s^0)\right] \quad [8]$$

where i_0 is given by Eq. 7 with $c_s = c_s^0$, c_s^0 is the initial surface concentration and $c_s^0 = c_p^0$ (assumption 8). In the linearized Butler–Volmer (BV) equation, the exchange current density is a function of the initial surface concentration, c_s^0. In this case, the perturbation voltage and the corresponding change in the surface concentration are given by

$$\tilde{V} = \phi_1 - \phi_2 - U_0 \quad [9]$$

and

$$\tilde{c}_s = c_{\text{surface}} - c_s^0 \quad [10]$$

The total current density of the particle is a sum of the faradaic and nonfaradaic current densities

$$j_n = j_{n,f} + C_{dl}\frac{\partial(\phi_1 - \phi_2)}{\partial t} \quad [11]$$

We refer to the model equation set (Eq. 1-3) with the faradaic current density represented by the linearized BV and the same equation set (Eq. 1-3) with the nonlinear BV equation (as given by Eq. 4) as the linear model and the nonlinear model, respectively.

Laplace Domain Solution for the Concentration

For a sinusoidal voltage input perturbation of frequency ω in radians

$$\tilde{V} = V\cos(\omega t) \quad [12]$$

the faradaic current density becomes a function of input perturbation (as per Eq. 8, 9, and 12). We know that the frequency ω in radians can be written in terms of the frequency, f, in Hz as $\omega = 2\pi f$. The set of mathematical equations (Eq. 1-3) describing the concentration gradients within the particle becomes a second-order partial-differential equation with a time-dependent boundary condition. This equation set can be solved for the surface concentration ($\tilde{c}_s$) after substituting $\tilde{c}_p = c_p - c_p^0$ (c_p^0 is the initial concentration in the particle), using the Laplace transformation technique to yield[1,9]

$$\tilde{c}_s(s) = -\frac{j_{n,f}(s)R_s}{D_sFY_s} \quad [13]$$

where

$$Y_s = \left(\frac{\sqrt{s\frac{R_s^2}{D_s}} - \tanh\left(\sqrt{s\frac{R_s^2}{D_s}}\right)}{\tanh\left(\sqrt{s\frac{R_s^2}{D_s}}\right)}\right) \quad [14]$$

and s is the Laplace variable.

The faradaic current density in the Laplace domain is obtained from Eq. 8 after substituting Eq. 12

$$j_{n,f}(s) = \frac{ni_0F}{RT}\left[\tilde{V}(s) + \left(-\frac{\partial U}{\partial c_s}\right)\Big|_{c_s^0,U}\tilde{c}_s(s)\right] \quad [15]$$

where based on Eq. 12

$$\tilde{V}(s) = \frac{Vs}{s^2 + \omega^2} \quad [16]$$

Replacing the expression for $j_{n,f}(s)$ in Eq. 14 with Eq. 15 and simplifying yields the perturbed surface concentration as a function of the applied voltage as

$$\tilde{c}_s(s) = -\frac{R_s}{D_s F}\frac{\tilde{V}(s)}{(R_{ct}Y_s + R_{part})} \quad [17]$$

where

$$R_{ct} = \frac{RT}{i_0 nF} \quad [18]$$

and

$$R_{part} = \left(-\frac{\partial U}{\partial c_s}\right)\Bigg|_{c_s^0,U}\frac{R_s}{FD_s} \quad [19]$$

and Y_s is given by Eq. 14.

Equation 17 can be used to obtain the periodic steady-state concentration in the time domain $[\tilde{c}_{s,ss}(t,\omega)]$ and the complete solution for the concentration domain that includes the initial transients also in the time domain $[\tilde{c}_s(t,\omega)]$. Each of the solutions can then be used along with Eq. 11 to obtain the periodic steady-state response current density $[j_{n,ss}(t,\omega)]$ and the complete expression for the response current density, including the initial transients $[j_n(t,\omega)]$. In the next two sections we describe the procedure used to obtained the two current responses, $j_{n,ss}(t,\omega)$ and $j_n(t,\omega)$.

Periodic Steady-State Current Response

The periodic steady-state solution to the equation set in Eq. 1-3, after it has been rewritten in terms of the perturbation variables $(\tilde{c}_p)$ can be derived in four steps.[32,33] First, assume that the input perturbation $\tilde{V}$ and the resulting gradients in $\tilde{c}_p$ are in periodic steady state and are complex. That is

$$\tilde{V} = V\exp(j\omega t) \quad [20]$$

and

$$\tilde{c}_s = \tilde{C}\exp(j\omega t) \quad [21]$$

where $j = \sqrt{-1}$ and $\tilde{C}$ is complex quantity. In the second step, substitute Eq. 20 and 21 into the governing equation and the boundary conditions. The resulting set of equations can be solved for $\tilde{c}_p$ at the surface to yield an analytical expression for $\tilde{C}$. As the third step, the periodic solution for the perturbed concentration with a complex input perturbation is obtained as a function of time and frequency, ω, by multiplying $\tilde{C}$ with $\exp(j\omega t)$. The resulting expression is a complex function. The final step consists of the determination of the periodic steady-state solution for the perturbed concentration corresponding to the assumed input perturbation. The final solution is obtained by taking the real part of the complex solution obtained in the previous step because we assumed the input perturbation to be $V\cos(\omega t)$. Then

$$\tilde{c}_{s,ss} = Re[\tilde{C}\exp(j\omega t)] \quad [22]$$

where

$$\tilde{C}\exp(j\omega t) = -\frac{R_s}{D_s F}\frac{V\exp(j\omega t)}{[R_{ct}Y_s(j\omega) + R_{part}]} \quad [23]$$

with $Y_s(j\omega)$ given by Eq. 14 after substituting $s = j\omega$. However, if the input perturbation is assumed to be $V\sin(\omega t)$, the final solution should be the imaginary part of the complex solution.

Another alternative procedure to derive the periodic steady-state solution is similar to the procedure described above. The only difference is in the second and third step. Instead of using the two steps as described above to determine the complex periodic solution, one can directly solve for the perturbed concentration at the surface using Laplace transformation by substituting the input perturbation voltage in the Laplace domain equal to a constant, the constant being equal to the amplitude of the input perturbation of interest. Next, replace $s = j\omega$ and multiply the resulting expression by $\exp(j\omega t)$. Comparing the two procedures, one can see that they differ only in the basic methodology of converting a partial-differential equation (PDE) to an ordinary-differential equation (ODE). The procedure described in the previous paragraph uses the complex variables introduced in Eq. 20 and Eq. 21, while the alternate procedure described in this paragraph uses the Laplace variable s, which is equal to $j\omega$ in the frequency domain, to convert the PDE to an ODE.

Either of the procedures described above can be used to determine the periodic steady-state expression for the perturbed surface concentration $[\tilde{c}_{s,ss}(t,\omega)]$ to obtain the periodic steady-state solution for the perturbed surface concentration, as given in Eq. 22. The corresponding periodic steady-state current density is given by

$$j_{n,ss}(t,\omega) = \frac{1}{R_{ct}}\left[\tilde{V}(t,\omega) + \left(-\frac{\partial U}{\partial c_s}\right)\Bigg|_{c_s^0,U}\tilde{c}_{s,ss}(t,\omega)\right] + C_{dl}\frac{\partial \tilde{V}(t,\omega)}{\partial t} \quad [24]$$

Current Response Including Initial Transient

The complete solution for the concentration in the time domain that includes the initial transient $[\tilde{c}_s(t,\omega)]$ can be derived by determining the Laplace inverse of Eq. 17. The solution presented in this section is an extension of the work published by Subramanian and White[13] for time-dependent current density. Equation 17 can be rewritten as the product of two Laplace functions

$$\tilde{c}_s(s) = G(s)F(s) \quad [25]$$

where

$$G(s) = \frac{R_s V_s}{D_s F(s^2 + \omega^2)} \quad [26]$$

and

$$F(s) = -\frac{\tanh(\sqrt{st_d})}{[R_{ct}\sqrt{st_d} + (R_{part} - R_{ct})\tanh(\sqrt{st_d})]} \quad [27]$$

In Eq. 27, t_d is defined as the diffusion time constant, which is equal to R_s^2/D_s. The Laplace inverse of Eq. 25 can be determined using the convolution theorem as

$$\tilde{c}_s(t,\omega) = \int_0^1 G(\tau)F(t-\tau)d\tau \quad [28]$$

when $G(t)$ and $F(t)$ are known. $G(t)$ is a straightforward solution

$$G(t) = L^{-1}[G(s)] = \frac{R_s V}{D_s F}\cos(\omega t) \quad [29]$$

The function $F(s)$ can be written as the ratio of two polynomials $P(s)$ and $Q(s)$

$$F(s) = \frac{P(s)}{Q(s)} = \frac{-1 + \frac{(t_d s)^3}{3} - \frac{2(t_d s)^5}{15} + \ldots}{R_{part} + \frac{(R_{ct} - R_{part})(t_d s)^3}{3} - \frac{2(R_{ct} - R_{part})(t_d s)^5}{15} + \ldots} \quad [30]$$

where the degree of $Q(s)$ is equal to the degree of $P(s)$. However, to obtain the Laplace inverse using the Heaviside expansion theorem, we know that the degree of $Q(s)$ must be greater than that of $P(s)$. To get around this problem, we first divide Eq. 27 by s, which yields the function $F(s)/s$ with the degree of the numerator greater than the denominator. Now the Laplace inverse of $F(s)/s$ can be determined using Heaviside expansion theorem as a function of time (t). The Laplace inverse of $F(s)/s$ thus determined is equivalent to $\int_0^t F(t)dt$. The Laplace inverse function is further differentiated with respect to

time, t, to get the required function $F(t)$. The methodology briefed here is demonstrated in detail in the next few equations. To begin with, dividing Eq. 27 by s, we get

$$L\left[\int_0^t F(t)dt\right] = \frac{F(s)}{s} = -\frac{\tanh(\sqrt{st_d})}{s(R_{ct}\sqrt{st_d} + (R_{part} - R_{ct})\tanh(\sqrt{st_d}))} \quad [31]$$

where $L[\ ]$ represents the Laplace transform of the function within the square brackets. Now, Eq. 31 can be inverted using Heaviside expansion theorem to yield

$$\int_0^t F(t)dt = L^{-1}\left[\frac{F(s)}{s}\right] = -\frac{1}{R_{part}} + \sum_{n=1}^{\infty} A_n \exp\left(-\frac{\lambda_n^2}{t_d}t\right) \quad [32]$$

where $L^{-1}[\ ]$ represents the Laplace inverse of the function within the square brackets

$$A_n = \frac{2\tan(\lambda_n)}{(R_{ct} - R_{part})\tan(\lambda_n)(\lambda_n\tan(\lambda_n) + 2) - \lambda_n(R_{ct} + R_{part})} \quad [33]$$

and λ_n for $n = 1 \ldots \infty$ are the roots of the equation

$$\lambda_n\cot(\lambda_n) = 1 - \frac{R_{part}}{R_{ct}} \quad [34]$$

$F(t)$ is given by

$$F(t) = \frac{d\left(\int_0^t F(t)dt\right)}{dt} \quad [35]$$

provided $F(0) = 0$. In this case, we know that $\tilde{c}_s(0,\omega) = 0$ (based on the initial condition) and $G(0)$= constant (see Eq. 29). Hence, $F(0)$ should be equal to zero and Eq. 35 is valid, yielding

$$F(t) = -\sum_{n=1}^{\infty} A_n \frac{\lambda_n^2}{t_d} \exp\left(-\frac{\lambda_n^2}{t_d}t\right) \quad [36]$$

where A_n is given by Eq. 33. Substituting Eq. 36 and 29 into Eq. 28, we get the complete solution for the perturbed surface concentration including the initial transients

$$\tilde{c}_s(t,\omega) = \frac{R_s V}{FD_s}\sum_{n=1}^{\infty}\left\{-\frac{A_n\lambda_n^2[\lambda_n^2\cos(\omega t) + \omega t_d\sin(\omega t)]}{[\lambda_n^4 + (\omega t_d)^2]} + \frac{A_n\lambda_n^4}{[\lambda_n^4 + (\omega t_d)^2]}\exp\left(-\frac{\lambda_n^2}{t_d}t\right)\right\} \quad [37]$$

Using Eq. 11, the response current density, including the initial transients, is given by

$$j_n(t,\omega) = \frac{1}{R_{ct}}\left[\tilde{V}(t,\omega) + \left(-\frac{\partial U}{\partial c_s}\right)\Big|_{c_s^0,U}\tilde{c}_s(t,\omega)\right] + C_{dl}\frac{\partial \tilde{V}(t,\omega)}{\partial t} \quad [38]$$

where $\tilde{c}_s(t,\omega)$ is given by Eq. 37.

Results and Discussion

Figure 2 gives the plot of the response current density solved numerically, response current density plotted using Eq. 38, and the periodic steady-state current density plotted using Eq. 24 at a frequency of $f = 0.1$ Hz. The numerical solution to the linear model is solved using the finite-element-based software package, Femlab. The parameter values used to construct the plot are given in Table I. The initial concentration is written as initial state charge, θ_0, defined by Eq. 5, where c_s is replaced with c_s^0. From Fig. 2, it is clear that the analytical solution for the response current density agrees well

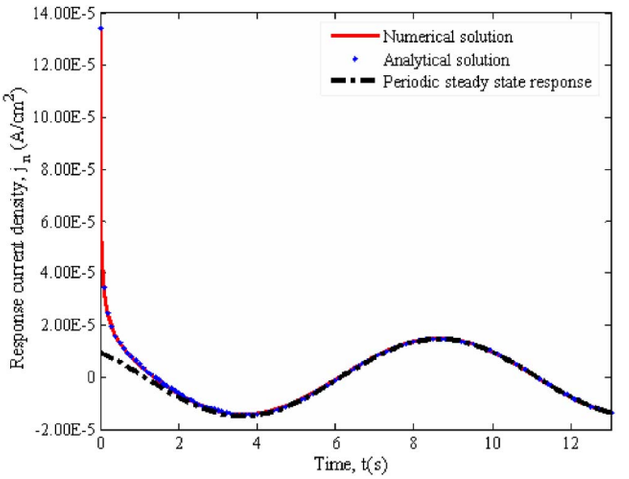

Figure 2. (Color online) Plot of the response current density obtained numerically and analytically and the steady-state current response as a function of time at frequency, $f = 0.1$ Hz. The number of terms in the analytical solution, $N = 1.00$.

with that of the numerical solution and the periodic steady-state solution agrees with the complete solution for the current response at long times. However, the number of terms used in the analytical solution for the response current density (Eq. 38) is too large (a few 1000 terms for $f = 0.01$ Hz). Even larger numbers of terms are required for simulating the response at higher frequencies. To get around this problem, we replace the periodic steady-state part of the complete solution for $\tilde{c}_s(t,\omega)$ (which is a series solution, Eq. 37) in the response with the periodic solution as obtained in Eq. 22 using complex variables. The periodic steady-state part of $\tilde{c}_s(t,\omega)$ is given by Eq. 37, neglecting the exponential term. Thus, the modified analytical solution for $\tilde{c}_s(t,\omega)$ becomes

$$\tilde{c}_s(t,\omega) = \frac{R_s V}{FD_s}\left\{\tilde{c}_{s,ss} + \sum_{n=1}^{\infty}\frac{A_n\lambda_n^4}{[\lambda_n^4 + (\omega t_d)^2]}\exp\left(-\frac{\lambda_n^2}{t_d}t\right)\right\} \quad [39]$$

$\tilde{c}_{s,ss}$ is given by Eq. 22, which is not a series solution. Through the modified perturbed-surface concentration expression, Eq. 39, the number of terms required for convergence is greatly reduced (maximum of 200 terms). We have already shown that $\tilde{c}_{s,ss}$ is equivalent to $\tilde{c}_s(t,\omega)$, given by Eq. 37, for long times in Fig. 2.

Nevertheless, the analytical solution depends on the roots of the transcendental equation Eq. 34, which is a function of the parameter values. The first ten values of the roots are tabulated (Table II) for

Table I. Parameter values obtained from the literature.

Parameter	Value	Source
k_a	6.9×10^{-4} A/cm^2	Ref. 30
c_{max}	0.0306 mol/cm^3	Ref. 30
c	0.001 mol/cm^3	Ref. 11
D_s	1.0×10^{-9} cm^2/s	Ref. 9
C_{dl}	1.0×10^{-5} F/cm^2	Ref. 9
R_s	2.0 μm	Ref. 9
θ_0	0.02302 mol/cm^3	assumed
$(-\partial U/\partial\theta)\|_{c_s^0,U}$	−20.27 V	Eq. 6
V	5.0 mV	See results and discussion section
i_0 (linear model)	6.9×10^{-4} A/cm^2	Eq. 7 calculated at initial conditions
R_{ct}	37.23 Ω cm^2	Eq. 18
R_{part}	1373.34 Ω cm^2	Eq. 19

Table II. Roots of the transcendental equation.

Number (n)	Lambda (λ_n)
1	3.05660030495913
2	6.11437916265974
3	9.17442157528053
4	12.2376430832104
5	15.3047432729875
6	18.3761916983703
7	21.4522413546693
8	24.5329604516116
9	27.6182726225610
10	30.7079976611546

the parameter values given in Table I. To solve for the roots numerically, appropriate initial conditions have to be provided, which again depend on the parameter values. Due to these reasons, it is difficult to use the analytical solution for parameter estimation, where the roots have to be determined many number of times, as when the parameter values are changed. In spite of this disadvantage associated with the analytical solutions, they can be very useful in gaining insight into the physics of the system and in evaluating limiting forms of the solution. Hence, we make use of both the numerical solution for the linear model in constructing plots and the analytical solution for certain analysis.

The amplitude of the input-voltage perturbation is chosen so that the average (averaged over four time periods, $4/f$) relative error of the response current density obtained using the linear model and the nonlinear model is less than 1%. The relative error is given by

$$\text{Relative error } (\%) = \frac{[j_{n,L}(t_i) - j_{n,NL}(t_i)]}{j_{n,NL}(t_i)} \times 100 \qquad [40]$$

where $j_{n,L}(t_i)$ and $j_{n,NL}(t_i)$ are the values of the response obtained using the linear model and nonlinear model, respectively, at time t_i. Note that the nonlinear model also has to be written in terms of the perturbed valuables. Writing the equations, Eqs. 1-3 and 8, in terms of the perturbed variables is straightforward. The BV equation in the boundary condition at $r = R_s$ in terms of the perturbed variables gives

$$j_{n,f} = i_0\left\{\exp\left[\frac{\alpha_a F}{RT}(\tilde{V} - \tilde{U})\right] - \exp\left[\frac{-\alpha_c F}{RT}(\tilde{V} - \tilde{U})\right]\right\} \qquad [41]$$

where $\tilde{V}$ is given by Eq. 9, $\tilde{U} = U - U_0$, which can be written as $f(\tilde{c}_s)$ using the known expression for the open-circuit potential (OCP) as a function of surface concentration, and i_0 in terms of the perturbed surface concentration is

$$i_0 = k\left[1 - \frac{(\tilde{c}_s + c_s^0)}{\tilde{c}_{\max}}\right]^{\alpha_n}\left(\frac{\tilde{c}_s + c_s^0}{c_{\max}}\right)^{\alpha_c} c_{\max}^{(\alpha_a+\alpha_c)} c^{\alpha_n} \qquad [42]$$

The nonlinear model was solved using the finite-element software package Femlab. The relative error for the response current density was below 1% for the amplitude value of 5 mV. Also, note that perturbed surface concentration, and in turn the response current density, are functions of the initial state of charge and initial slope of the OCP. Hence, it is important to check the validity of linearity of the OCP with respect to the state of charge should be ensured. This is because the empirical equations used to fit the experimentally measured nonlinear OCP curves may be inadequate at certain points, such as the region where the curve transitions from one voltage plateau to another. In such cases, the derivation of the OCP can be determined numerically instead of using the empirical equation as such. The OCP and its slope are plotted in Fig. 3 and 4. The abscissa in these figures is the state of charge. The values of the averaged relative error for the response current density and the averaged relative error for the perturbed surface concentration calculated for various values of the initial state of charge, θ_0, as indicated in Fig. 3 and 4 lie below the acceptable limit (1%).

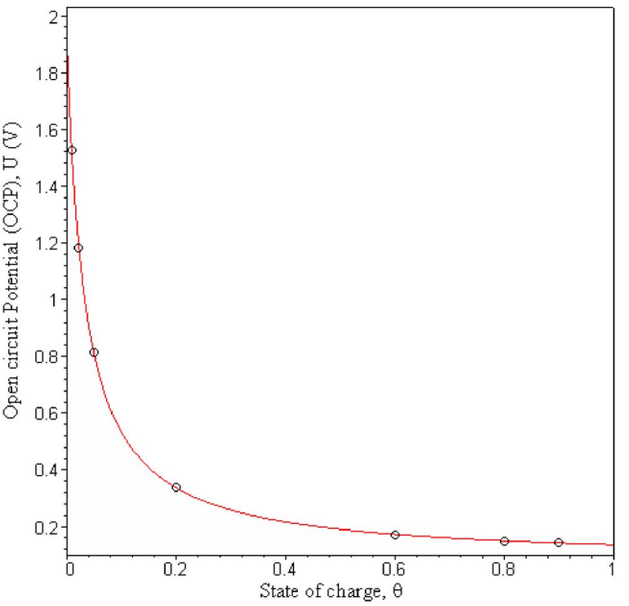

Figure 3. (Color online) Plot of the OCP as a function of state of charge.

Transient Analysis

In this section we first analyze the short-time response to investigate the information contained in it, similar to our previous work.[34] Even before we start analyzing the short-time response, it is necessary to clarify the definition of what we mean by short-time response. The short-time response is the time range over which the transient analysis is dominant. Now, the time range for short-time response is from 0 to the time constant for the transient response. The time constant for the transient response of this system can be

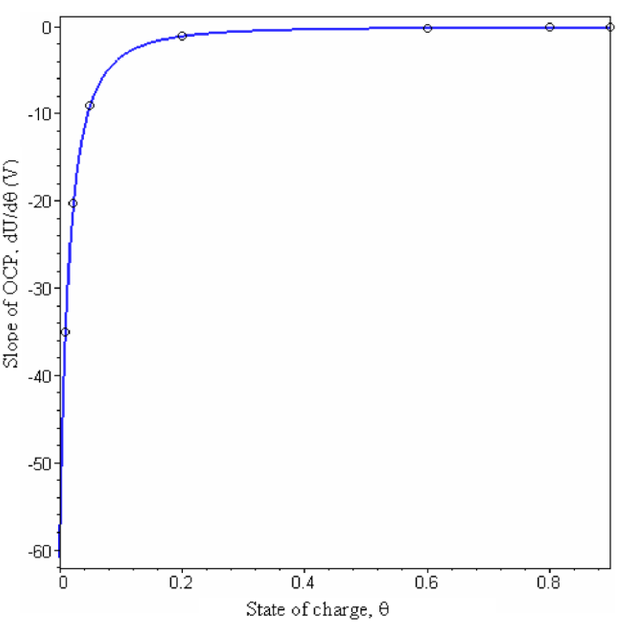

Figure 4. (Color online) Plot of the slope of the OCP as a function of state of charge.

extracted from the expression for the transient part of the analytical solution for the response current density, Eq. 38 with Eq. 37 (time constant appearing in the exponential term)

$$t_0 = t_d \sum_{n=1}^{\infty} \frac{1}{\lambda_n^2} \quad [43]$$

Note that the time constant t_0 does not depend on the double-layer charging process because the double layer is restricted only to the interface and is independent of other processes occurring in the system (see assumptions 3 and 4). Unlike the double-layer charging process, the other part of the response current density brought about by the interfacial reaction process is linked to the diffusion process in the particle and the diffusion process occurs due to the perturbed-concentration distribution in the particle. The perturbed concentration in the particle attains the periodic steady state (or the pseudo steady state) after an initial adjustment period, which gives rise to the transient response. This transient response in perturbed concentration is reflected in the interfacial reaction current density ($j_{n,f}$) because $j_{n,f}$ depends on the perturbed surface concentration (see Eq. 8).

In order to calculate the time constant t_0 according to Eq. 43, we need to evaluate the summation series with a finite number of terms. The number of terms in the series, as mentioned earlier, decreases with a decrease in the frequency. This gives rise to an increase in the time constant from zero time constant value (because at highest frequency no concentration exists) at highest frequencies to 6.97 s at low frequency ($f = 0.01$ Hz). Based on these values, the transient region is defined as the time scale between $t = 0$ s and $t = t_0$ s, where t_0 is a function of the frequency. Consider the coefficient of the exponential function in the transient part of the response (Eq. 38 with Eq. 37). The coefficient is inversely proportional to frequency and hence has a very small value at high frequencies. A small value for the coefficient of the exponential term combined with a higher value for the time constant leads to negligible transient response at higher frequencies. Another factor that has to be taken into account in analyzing the short-time response is that the double-layer charging current is directly proportional to the frequency of the applied perturbation. But, at time $t = 0$ both the double-layer charging current and faradaic current density due to the perturbed surface concentration go to zero (see Eq. 38 and 37). Consequently, at higher frequencies the short-time response is dominated by the interfacial kinetics and double-layer charging current and is equal to the periodic steady-state current because the transient response is negligible, while at low frequencies the short-time response is dominated by the interfacial kinetics combined with the diffusion process in the particle, leading to a significant contribution from the transient response. The results of the short-time analysis explained so far are illustrated in Fig. 5 and 6, and the limiting expressions for the response current density and its slope are

$$j_n\big|_{t=0} = \frac{V}{R_{\text{ct}}} \quad [44]$$

$$\left.\frac{dj_n}{dt}\right|_{t=0,\tilde{c}_s=0} = -V\omega^2 C_{\text{dl}} \quad [45]$$

$$\left.\frac{dj_n}{dt}\right|_{t=0,\omega=0} = \frac{R_{\text{part}} V}{R_{\text{ct}}} \sum_{n=1}^{\infty} \frac{-\lambda_n A_n}{t_d} \quad [46]$$

At very low frequencies the input perturbation is equivalent to a step input and hence, the response current density at low frequencies agrees with the response current density for a step input of step size equal to the amplitude of the sinusoidal signal. The response current density in this case is given by

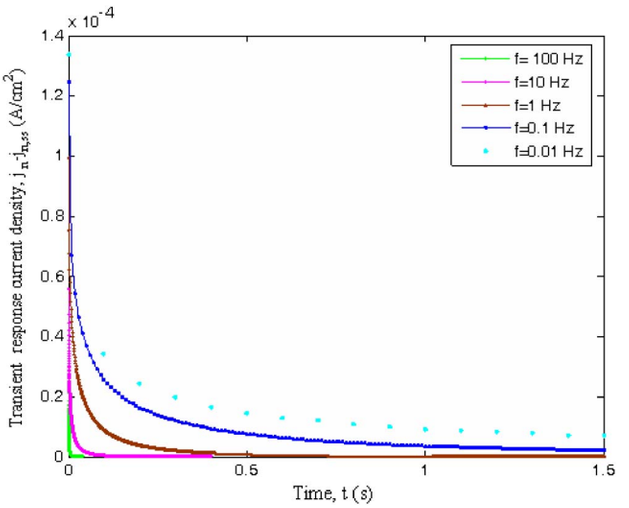

Figure 5. (Color online) Transient part of the response current density as a function of time at different values of the frequency.

$$j_n\big|_{\omega=0} = \frac{1}{R_{\text{ct}}}\left(\tilde{V}(t,\omega) + \left(-\frac{\partial U}{\partial c_s}\right)\Big|_{c_s^0,U} \times\left\{\frac{R_s V}{F D_s}\sum_{n=1}^{\infty}\left[-A_n + A_n \exp\left(-\frac{\lambda_n^2}{t_d}t\right)\right]\right\}\right) \quad [47]$$

The long-time periodic response, used in impedance analysis, contains similar information to that of the short-time response. Analysis of the periodic steady-state response can be performed by observing the change in the amplitude of the response, $j_{n,\text{amp}}$. Using the amplitude of the response current density, a variation of $V/j_{n,\text{amp}}$ that is equivalent to the magnitude of the impedance[1,9] as a function of frequency is shown in Fig. 7. The complex plane plot of the system can also be generated from the coefficient of the $\cos(\omega t)$ and $\sin(\omega t)$ term of the inverse of the periodic response.

Effect of parameters.— Similar to impedance that separates the different physical phenomenon involved in a system experimentally, sensitivity analysis is a mathematical tool that aids in separating the

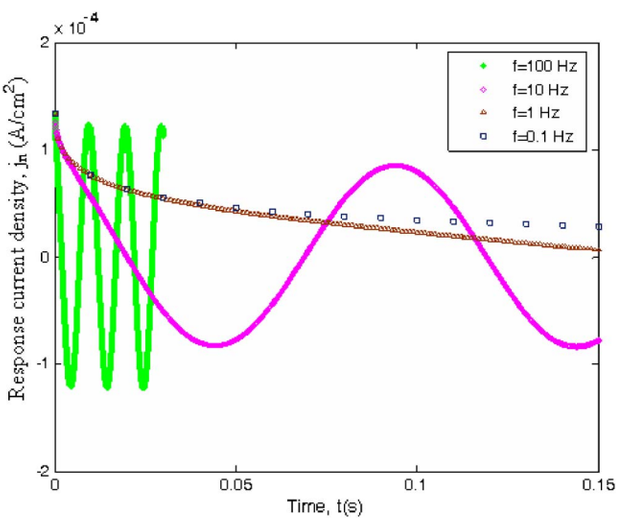

Figure 6. (Color online) Response current density at short-time periods for different frequency values.

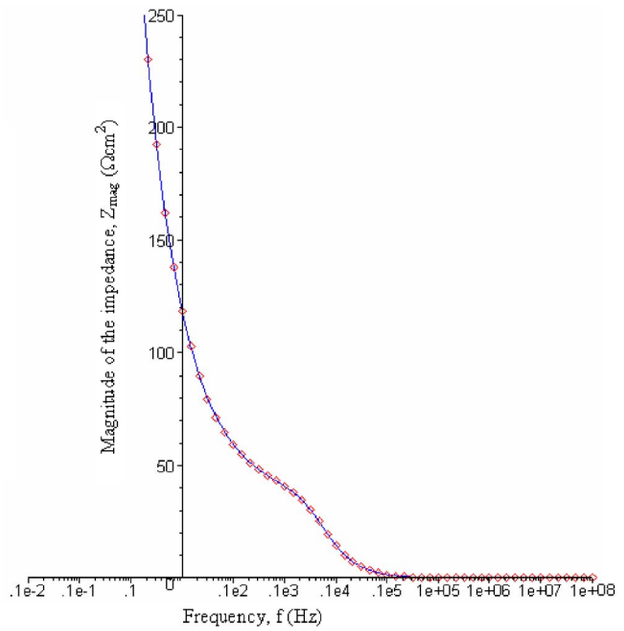

Figure 7. (Color online) Bode magnitude plot. Symbols are obtained from the ratio of the amplitude of the input perturbation, V, to the periodic response current density, $j_{n,ss}$. The magnitude of the impedance determined from the impedance expression is plotted as a line.

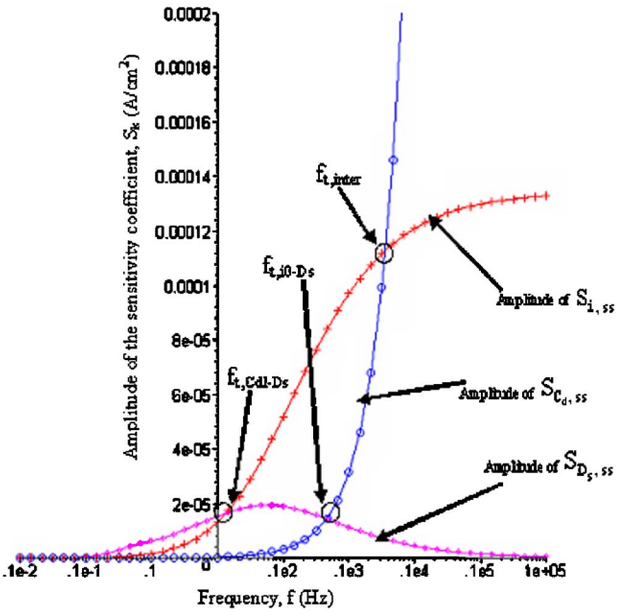

Figure 8. (Color online) Plot of the amplitude of the sensitivity coefficient of die exchange current density (i_0), double-layer capacitance (C_{dl}), and the diffusion coefficient (D_s) as a function of frequency.

physical processes. The sensitivity of the parameters to the total voltage response is calculated using the normalized sensitivity coefficients (S_{i_0}, $S_{C_{dl}}$, and S_{D_s}) of i_0, C_{dl}, and D_s, respectively, defined as[35]

$$S_k = k\frac{\partial j_n}{\partial k}; \quad k = j_0,\ C_{dl} \text{ or } D_s \qquad [48]$$

The normalization is with respect to the parameter and is performed to maintain consistent units for the sensitivity coefficients. The sensitivity coefficients are also periodic, similar to the response current density. The sensitivity of the parameters to the steady-state response (represented as $S_{k,ss}$) is obtained by plotting the sensitivity coefficients for longer time periods. The sensitivity of the parameters to the transient-voltage response (represented as $S_{k,t}$) can be determined by evaluating the same expression for very short time periods. Plot of the amplitude of the steady-state sensitivity coefficients as a function of time for various frequencies (see Fig. 8) gives insight into the physics. At higher frequencies the interfacial phenomenon dominates the response as the amplitude of the sensitivity coefficient of the double-layer capacitance and the exchange current density are high, while at very low frequencies the amplitude of $S_{k,ss}$ of the diffusion coefficient is the highest while the sensitivity of the parameters associated with the interfacial phenomenon are close to zero. Tracing the change in the sensitivity coefficients in the transient as a function of time (that is $S_{k,t}$) at a fixed value of the frequency where diffusion process is significant (see Fig. 9), shows that the sensitivity coefficient of the exchange current density is the highest at time $t = 0$ while the others are zero, which is expected due to Eq. 44. Also, the maximum value of the sensitivity for each of the parameters in the transient region is close (not equal) to that of the steady-state sensitivities. As the frequency is lowered, the $S_{k,t}$ value of the exchange current density and diffusion coefficient becomes higher than the periodic steady-state sensitivity values, though at time $t = 0$ the $S_{k,t}$ of the exchange current density retains the highest value.

At moderate frequencies, we see the crossover of the profiles of the amplitude of $S_{k,ss}$ for the parameters at certain frequencies (Fig. 8). The frequency at which the crossover occurs is called the transition frequency (f_t) in general. When the crossover is between the sensitivity profiles of parameters that are associated with the interfacial phenomenon, the transition frequency associated with interfacial phenomenon is denoted as $f_{t,inter}$. Similarly, two other transition frequencies occur in the amplitude of the $S_{k,ss}$ plot: the transition frequency associated with the diffusion and the interfacial kinetics, $f_{t,i0-Ds}$, and that associated with the diffusion and double-layer charging processes, $f_{t,Cdl-Ds}$. The values of these transition frequencies are indicated in Fig. 8. The transition frequency is a pointer that indicates the frequencies at which the system switches from one process to another to deliver the current density. According to the transition from one process to another, the sensitivity of the corre-

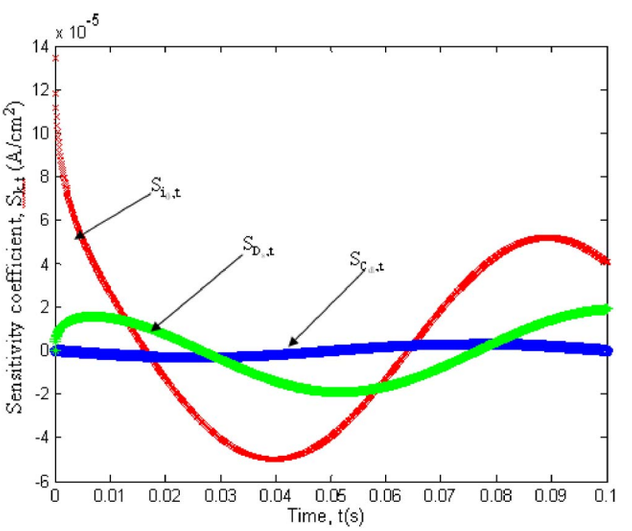

Figure 9. (Color online) Plot of the sensitivity coefficients of the parameters in the transient region at a frequency of 0.1 Hz as a function of time in the transient region.

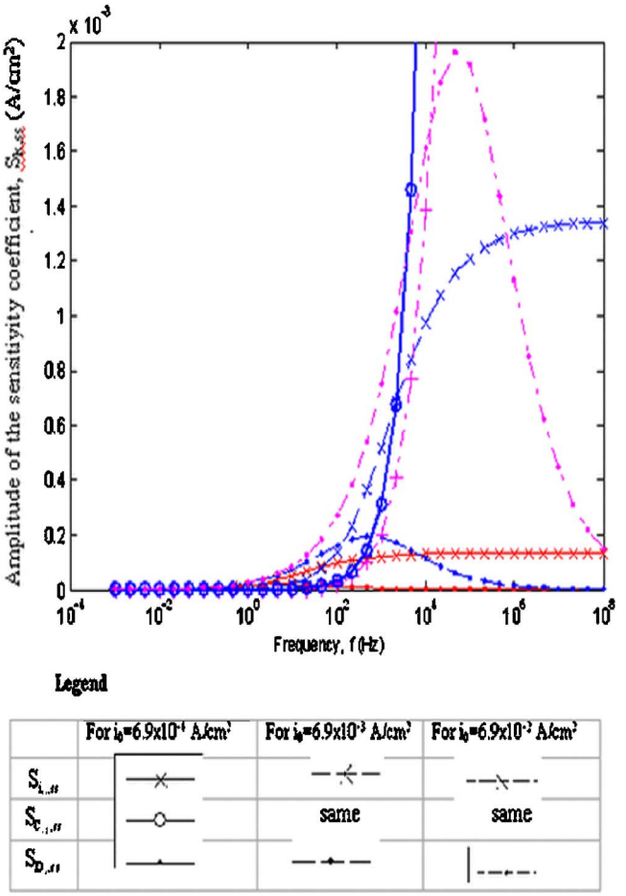

Figure 10. (Color online) Plot of the amplitude of the steady-state sensitivity coefficients of the parameters for different values of the exchange current density. The amplitude of the sensitivity coefficient of the double-layer capacitance is independent of j_0.

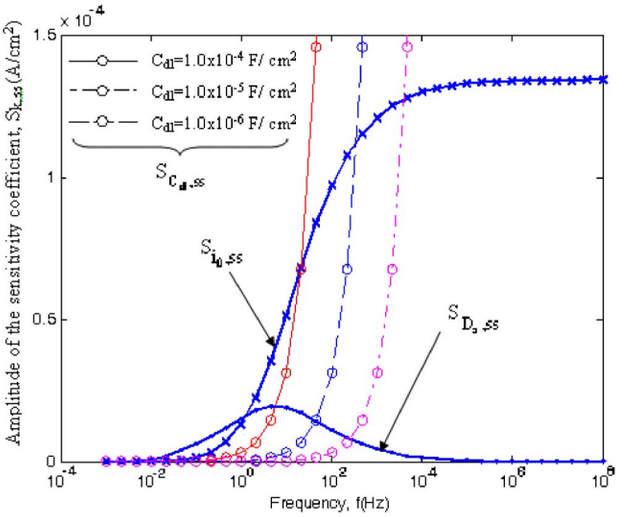

Figure 11. (Color online) Plot of the amplitude of the steady-state sensitivity coefficients of the parameters for different values of the double-layer capacitance. The change is only in the profile for the amplitude of the sensitivity coefficient of the double-layer capacitance. The legends are as indicated in the figure.

sponding parameters changes. This phenomenon is explained in detail with respect to Fig. 8. Beginning with very high frequencies, the double-layer charging process gives rise to the response current density. As the frequency is lowered, transition from the double-layer process to the interfacial reaction current occurs at frequencies lower than the transition frequency, $f_{t,\text{inter}}$, but higher than $f_{t,\text{Cdl}-Ds}$. However, at these frequencies the double-layer current is not zero and should be included to get the total response current density. Below the transition frequency, $f_{t,\text{Cdl}-Ds}$, the double-flayer charging current becomes very low, while there is significant current generated from the diffusion of ions in the particle apart from the current due to the interfacial reaction. This behavior is true for the transition frequency associated with the diffusion and interfacial reaction, $f_{t,i0-Ds}$. Below $f_{t,i0-Ds}$ the system switches from the interfacial reaction current density to the current density generated by the diffusion process. Meanwhile, the reaction current drops slowly.

The effect of parameter values can be studied based on the changes in the sensitivity profiles and the changes in the values of the transition frequencies. Sensitivity plots for different values of i_0, C_{dl}, and D_s are shown in Fig. 10-12, respectively. The values of the transition frequencies determined with a change in the parameter values are given in Table III. The transition frequencies can be calculated by equating the amplitudes of both the steady-state periodic processes and solving for the frequency, f. An increase in the value of the exchange current density pushes the sensitivity profiles of the exchange current density and the diffusion coefficient towards higher frequencies and they are scaled up in magnitude (see Fig. 9), but it does not have any influence on the sensitivity of the double-layer capacitance. The amplitude of the steady-state sensitivity coefficient for the double-layer capacitance is a simple expression, which is dependent on only the value of C_{dl} (see Fig. 9)

$$S_{C_{\text{dl}}} = -VC_{\text{dl}}\omega \sin(\omega t) \qquad [49]$$

Also, the value of the double-layer capacitance does not affect the sensitivities of the other two parameters (see Fig. 10). This is because the double-layer charging process is separated from both the interfacial kinetics and the concentration gradients in the particle. The transition frequencies, $f_{t,\text{Cdl}-Ds}$ and $f_{t,i0-Ds}$, are inversely proportional to the double-layer capacitance. The transition frequencies associated with diffusion coefficient, $f_{t,\text{inter}}$, $f_{t,\text{Cdl}-Ds}$, and $f_{t,i0-Ds}$, are directly proportional to D_s, inversely proportional to D_s, and not influenced by the value of D_s, respectively. From Fig. 11, we see that changing the diffusion coefficient does not affect the maximum value of the sensitivity of i_0 occurring at high frequencies, whereas the slope of the same in midfrequencies becomes steeper with an increase in its value. The peak value of the sensitivity of D_s does not change much with D_s, whereas the peak value is shifted towards a higher frequency as the value of D_s decreases, provided $D_s \leq 1 \times 10^{-9}$ cm^2/s. When $D_s > 1 \times 10^{-9}$ cm^2/s, there is a change in the peak frequency values as well as the frequency at which it occurs. The correlation between the parameters can also be studied from the change in the sensitivity plots. The sensitivity plots for the exchange current density (Fig. 12) do not change with the value of the diffusion coefficient above $f = 100$ kHz, with the exception of very low frequency values ($D_s = 1 \times 10^{-11}$ cm^2/s). However, the sensitivity plots for the diffusion coefficient (Fig. 10) are highly sensitive to the change in the value of the exchange current density throughout the whole frequency range.

Taking note of the change in the values of the transition frequencies with the parameters and relating it to the expressions for the time constants mentioned in the literature,[8] the following approximate expression is determined

$$f_{t,\text{inter}} \approx \frac{i_0 F}{C_{\text{dl}} \text{RT}} \qquad [50]$$

Parameter estimation.— Based on the analysis of short-time response and sensitivity analysis, we can conclude that the parameters

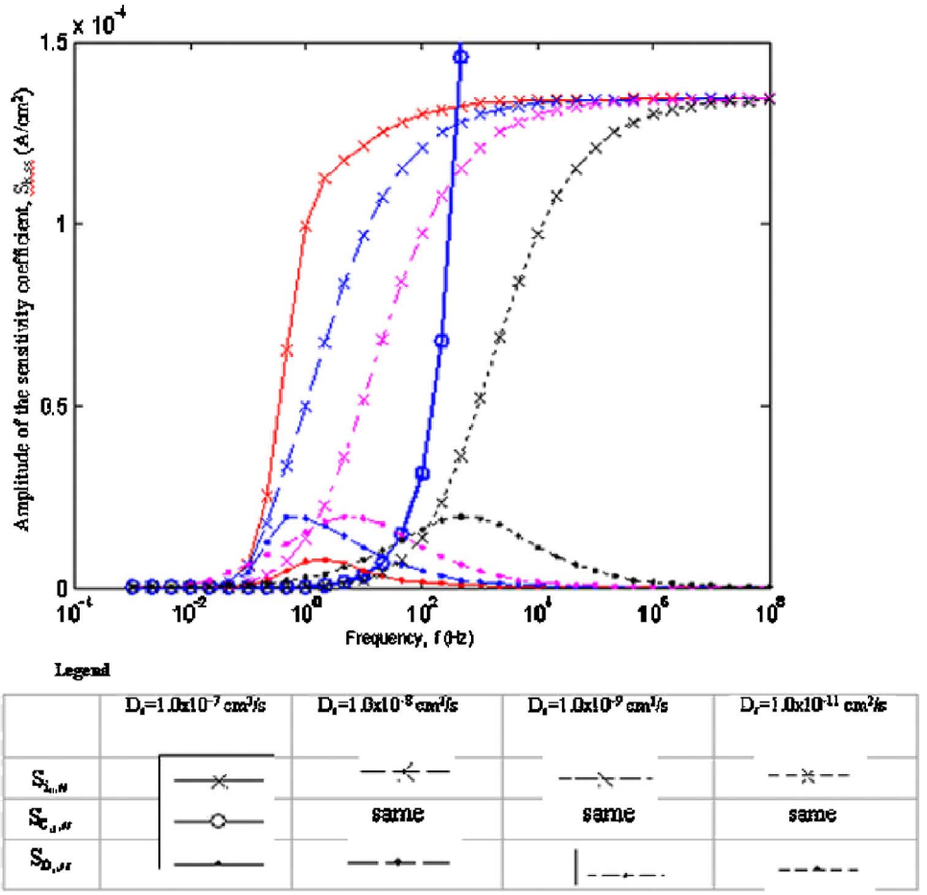

Figure 12. (Color online) Plot of the amplitude of the steady-state sensitivity coefficients of the parameters for different values of the diffusion coefficient. The amplitude of the sensitivity of the double-layer capacitance is independent of D_s.

of the system can be determined sequentially from the response in the transient region obtained at higher to lower frequencies. The inclusion of the transient response enables us to determine the value of the exchange current density even with data at low frequencies, which is otherwise not possible with the periodic steady-state data. Combining the ability to determine i_0 from the voltage response at time $t = 0$ to the fact that the double-layer process dominates the response at high frequencies, the parameter values of i_0 and C_{dl} can be determined. The diffusion coefficient can be determined by sequentially fitting the transient data from high frequency followed by low frequency. High-frequency value is the frequency in the kHz range or higher. Selection of the low-frequency value can be made based on the value of C_{dl} or with C_{dl} and i_0. In general, the low-frequency value can be (*i*) the transition frequency of the interfacial process calculated using Eq. 50 or (*ii*) the frequency at which the amplitude of the sensitivity of the double-layer capacitance is equal to or lower than one-tenth of the value of C_{dl} itself.

Table III. Crossover frequencies for various parameter values.

Parameter changed	Parameter value	$f_{t,\text{inter}}$ (Hz)	$f_{t,\text{Cdl}-Ds}$ (Hz)	$f_{t,i0-Ds}$ (Hz)
Base values	-	359.64	45.76	1.35
i_0	6.9×10^{-3}	2192.16	624.45	135.27
(A/cm^2)	6.9×10^{-2}	-NA-	3971.50	13528.0
C_{dl}	100	21.85	6.19	1.35
(F/cm^2)	1	4059.56	254.05	1.35
D_s	1×10^{-7}	420.67	12.86	-NA-
(cm^2/s)	1×10^{-8}	405.95	25.40	-NA-
	1×10^{-11}	-NA-	39.72	1.35

In order to extract the diffusion coefficient more reliably, the following procedure that uses parameter estimates at more than one frequency could be adopted:

1. The estimates of i_0, C_{dl}, and D_s are determined from data at high frequencies (in kHz).
2. The estimates obtained at this frequency can be used to determine $f_{t,\text{inter}}$, and the values for the parameters obtained previously can be the initial guess values for the parameter estimation process at $f_{t,\text{inter}}$.
3. The estimates from the previous step ($f = f_{t,\text{inter}}$) can be used as the initial guess values for the parameter estimation at the other low-frequency value mentioned earlier (the frequency at which the amplitude of the sensitivity of the double-layer capacitance is equal to or lower than one-tenth of the value of C_{dl}). The parameter estimation at this frequency is only carried out for the parameters i_0 and D_s due to the obvious choice of the frequency.
4. The final estimates for i_0 is the average of the estimates obtained at two lower frequencies, while for the estimate of C_{dl} and diffusion coefficient are the average of the values obtained at the first two frequencies (high f and $f_{t,\text{inter}}$) and two lower frequency values, respectively.

Getting the parameters using the estimates at more than one frequency is a more foolproof method than the estimates obtained at just one frequency. Parameter estimates using this procedure have been determined by optimizing the error between the model results against synthetic data. The Matlab optimization function *Isqcurvefit*, with bounds set on the parameter values so that they are positive values, was employed. The set values and estimates along with their confidence intervals calculated at various frequencies are shown in

Table IV. Parameter estimates for three different cases obtained at three different frequencies. The sampling frequency for the data at frequencies of 10 kHz, $f_{t,\text{inter}}$, and 3.183 Hz are 0.1 GHz, 100 kHz, and 10 kHz, respectively.

Case no.	Parameter	Set parameter values	Parameter estimates: At high frequency (f = 10 kHz)	Parameter estimates: At $f = f_{t,\text{inter}}$	Parameter estimates: At f = 3.183 Hz
1	i_0 (A/cm^2)	6.9×10^{-4}	$(7.1003 \pm 2.251) \times 10^{-4}$	$(6.819 \pm 0.265) \times 10^{-4}$	$(6.862 \pm 0.0395) \times 10^{-4}$
	C_{dl} (F/cm^2)	1.0×10^{-5}	$(1.002 \pm 0.0135) \times 10^{-5}$	$(1.0113 \pm 0.0349) \times 10^{-5}$	—
	D_s (cm^2/s)	1.0×10^{-8}	$(0.117 \pm 547.14) \times 10^{-8}$	$(3.822 \pm 27.19) \times 10^{-8}$	$(1.026 \pm 0.0368) \times 10^{-8}$
2	i_0 (A/cm^2)	6.9×10^{-4}	$(6.929 \pm 1.62) \times 10^{-4}$	$(6.714 \pm 0.425) \times 10^{-4}$	$(6.818 \pm 0.3815) \times 10^{-4}$
	C_{dl} (F/cm^2)	1.0×10^{-5}	$(0.999 \pm 0.0079) \times 10^{-5}$	$(1.008 \pm 0.012) \times 10^{-5}$	—
	D_s(cm^2/s)	1.0×10^{-11}	$(2.0283 \pm 4.88) \times 10^{-11}$	$(1.048 \pm 0.1224) \times 10^{-11}$	$(1.0013 \pm 0.0503) \times 10^{-11}$
3	i_0 (A/cm^2)	6.9×10^{-4}	$(7.435 \pm 1.525) \times 10^{-4}$	$(6.908 \pm 0.104) \times 10^{-4}$	$(6.896 \pm 0.0398) \times 10^{-4}$
	C_{dl} (F/cm^2)	1.0×10^{-5}	$(0.995 \pm 0.0076) \times 10^{-5}$	$(1.0102 \pm 0.0336) \times 10^{-5}$	—
	D_s (cm^2/s)	1.0×10^{-7}	$(1.752 \pm 3.308) \times 10^{-11}$	$(0.4509 \pm 2.61) \times 10^{-7}$	$(1.001 \pm 0.112) \times 10^{-7}$

Table IV. Three different cases were considered: (*i*) both diffusion and interfacial reaction are important, (*ii*) diffusion-limited, and (*iii*) interfacial-phenomenon-limited. The length of time over which data is required for parameter estimation is chosen to be half the cycle length at which one is operating. For example, if we are interested in the parameter estimation at a frequency, f, the length of the data required would be until the end time $t = T_{\text{end}}$, given by

$$T_{\text{end}} = \frac{1}{2f} \quad [51]$$

The sampling frequency (f_s) was chosen so that enough data points could be recorded within the time limit, which ensures quick estimates of the parameters. The sampling frequency for the data at frequencies of 10 kHz, $f_{c,\text{inter}}$, and 3.183 Hz are 0.1 GHz, 100 kHz, and 10 kHz, respectively. The data length, which is a product of end time and sampling frequency ($T_{\text{end}}xf_s$), can be calculated when the operating frequencies are known. Synthetic data is generated by adding random noise to the simulated results. The standard deviation of the noise is calculated based on the assumed value of the signal-to-noise (SN) ratio with respect to the amplitude of the response

$$\text{SN(in dB)} = 20 \log_{10}\left(\frac{A_{\text{response}}}{A_{\text{noise}}}\right) \quad [52]$$

where A_{response} is the amplitude of the current density response and A_{noise} is the standard deviation of the noise applied. The above equation can be used to determine A_{noise} assuming that SN = −70 dB. The final estimates for the parameters with the associated confidence intervals, resulting from the average of the parameters obtained at different frequencies, are presented in Table V. Note that narrow confidence intervals indicate that the parameter estimates are trustworthy. Good estimates for cases 1 and 2 were obtained, while the estimate for the diffusion coefficient for the case where the system is kinetic limited the value of the diffusion coefficient and is accurate only at f = 3.183 Hz. The estimate for the exchange current density and double-layer capacitance is good for case 3. The associated confidence intervals calculated for the parameters further certify the accuracy of the parameter values. Note that the lowest frequency used for parameter estimation is about 3 Hz and the time required to measure the data at this frequency amounts to 0.17 s (from Eq. 51). Hence, the maximum experimental time for the short-time analysis for parameter estimation is in the milliseconds, making the technique fast and accurate.

Table V. Final averaged parameter estimates for the three cases and the values of the transition frequency $f_{t,\text{inter}}$ used.

Case no.	$f_{t,\text{inter}}$ (Hz)	Final parameter estimates
1	430	$i_0 = (6.841 \pm 0.152) \times 10^{-4}$ A/cm^2
		$C_{\text{dl}} = (1.005 \pm 0.0242) \times 10^{-5}$ F/cm^2
		$D_s = (1.026 \pm 0.0368) \times 10^{-8}$ cm^2/s
2	430	$i_0 = (6.766 \pm 0.4035) \times 10^{-4}$ A/cm^2
		$C_{\text{dl}} = (1.003 \pm 0.010) \times 10^{-5}$ F/cm^2
		$D_s = (1.025 \pm 0.0864) \times 10^{-11}$ cm^2/s
3	462	$i_0 = (6.902 \pm 0.0719) \times 10^{-4}$ A/cm^2
		$C_{\text{dl}} = (1.002 \pm 0.0206) \times 10^{-5}$ F/cm^2
		$D_s = (1.001 \pm 0.112) \times 10^{-7}$ cm^2/s

Conclusion

The model equations for the intercalation particle are solved for the periodic steady-state solution as well as the complete solution, including the initial transients. The response of the complete solution in the transient region (short-time response) is analyzed with the aim to estimate the parameters of the system. The parameters are exchange current density, double-layer capacitance, and the solid-phase diffusion coefficient. The results presented here confirm that the information contained in the periodic steady-state response is accessible by analyzing just the short-time response. Sensitivity analysis provides more insight into the physics and the distribution of the processes in the frequency domain and hence is used to study the effect of the parameters on the response. The analysis is also used to develop a methodology to estimate parameters sequentially using data of the current-density response at more than one frequency of the input perturbation. Accurate values for the parameters can be obtained at a faster rate because the response at short times (a few milliseconds) is used to estimate the parameters.

University of South Carolina assisted in meeting the publication costs of this article.

List of Symbols

A_n	see Eq. 33
c	concentration in the solution phase, mol/cm^3
c_{max}	maximum concentration in the particle, mol/cm^3
c_p	concentration in the particle, mol/cm^3
c_s	surface concentration, mol/cm^3
C_{dl}	double-layer capacitance, F/cm^2
D_s	diffusion coefficient, cm^2/s
f	frequency, Hz (1/s)
f_s	sampling frequency, Hz
f_t	transition frequency, Hz
F	Faraday's constant, 96487 C/mol
j_n	response current density, A/cm^2
$j_{n,\text{ss}}$	periodic steady-state response current density, A/cm^2
i_0	exchange current density, A/cm^2 (see Eq. 7)
$j_{n,f}$	faradaic interfacial current density, A/cm^2
k_a	reaction rate of the intercalation electrode, A/cm^2/(mol/cm^3)$^{3/2}$
$L[\ ]$	Laplace transform of the function within the square brackets
$L^{-1}[\ ]$	Laplace inverse of the function within the square brackets
n	number of electrons transferred in the reaction, (=1)

r	radial distance, cm
R	universal gas constant, 8.313 J/mol K
R_{ct}	see Eq. 18, Ω cm^2
R_{part}	see Eq. 19, Ω cm^2
R_s	particle radius, cm
T	temperature, K
t	time, s
t_d	time constant for diffusion process, s(R_s^2/D_s)
T_{end}	time limit for synthetic data operated at a particular frequency, s (see Eq. 51)
U	OCP, V (see Eq. 6)
V	amplitude of the applied-voltage density, V
$\tilde{V}$	perturbed voltage applied to the particle, $V\cos(\omega t)$, V
S_k	normalized sensitivity coefficient of the parameter, k, V (see Eq. 48)
SN	signal-to-noise ratio, dB (see Eq. 52)
$(-\partial U/\partial c_s)\|_{3}$	slope of the OCP with respect to surface concentration at the initial conditions, Vcm^3/mol
Z_{mag}	magnitude of the impedance (Ω cm^2)

Greek

α_a, α_c	anodic and cathodic transfer coefficients, respectively ($\alpha_a + \alpha_c = n$)
ϕ_1	solid phase potential, V
ϕ_2	solution phase potential, V
η	overpotential ($\phi_1 - \phi_2$), V
λ_n	nth root of the transcendental equation, Eq. 34
θ	state of charge, see Eq. 5
ω	frequency of the applied current, rad/s($=2\pi f$)

Subscripts

0	initial value of the variable
ss	variable in steady state region
t	variable in the transient region
$\sim$	perturbed variable

Superscripts

0	initial value of the variable

References

1. B. S. Haran, B. N. Popov, and R. E. White, *J. Power Sources*, **75**, 56 (1998).
2. P. M. Gomadam, J. W. Weidner, R. A. Dougal, and R. E. White, *J. Power Sources*, **110**, 267 (2002).
3. A. Hjelm, G. Lindbergh, and A. Lundqvist, *J. Electroanal. Chem.*, **506**, 82 (2001).
4. M. Umeda, K. Dokko, Y. Fujita, M. Mohamedi, I. Uchida, and J. R. Selman, *Electrochim. Acta*, **47**, 885 (2001).
5. M. Dokko, M. Mohamedi, M. Umeda, and I. Uchida, *J. Electrochem. Soc.*, **150**, A425 (2003).
6. M. Dokko, M. Mohamedi, Y. Fujita, T. Itoh, M. Nishizawa, M. Umeda, and I. Uchida, *J. Electrochem. Soc.*, **148**, A422 (2001).
7. I. Uchida, M. Mohamedi, K. Dokko, M. Nishizawa, T. Itoh, and M. Umeda, *J. Power Sources*, **97–98**, 518 (2001).
8. D. Zhang, B. N. Popov, and R. E. White, *J. Electrochem. Soc.*, **147**, 831 (2000).
9. J. P. Meyers, M. Doyle, R. M. Darling, and J. Newman, *J. Electrochem. Soc.*, **147**, 2930 (2000).
10. G. Ning and B. N. Popov, *J. Electrochem. Soc.*, **151**, A1584 (2004).
11. S. Santhanagopalan, Q. Guo, P. Ramadass, and R. E. White, *J. Power Sources*, In press.
12. A. V. Oppenheim and R. W. Schafer, *Digital Signal Processing*, Prentice Hall, Englewood Cliffs, NJ (1975).
13. V. Subramanian and R. E. White, *J. Power Sources*, **96**, 385 (2001).
14. S. Liu, *Solid State Ionics*, **177**, 53 (2006).
15. S. Motupally, C. C. Streinz, and J. W. Weidner, *J. Electrochem. Soc.*, **142**, 1401 (1995).
16. B. S. Haran, B. N. Popov, and R. E. White, *J. Power Sources*, **75**, 56 (1998).
17. P. Arora, B. N. Popov, and R. E. White, *J. Electrochem. Soc.*, **145**, 807 (1998).
18. A. Lundquist and G. Lindbergh, *Electrochim. Acta*, **44**, 2523 (1999).
19. P. Yu, B. N. Popov, J. A. Ritter, and R. E. White, *J. Electrochem. Soc.*, **146**, 8 (1999).
20. Q. Guo, V. R. Subramanian, J. W. Weidner, and R. E. White, *J. Electrochem. Soc.*, **149**, A307 (2002).
21. Y. Chang, J. Jong, and G. T. Fey, *J. Electrochem. Soc.*, **147**, 2033 (2000).
22. M. Doyle, J. P. Meyers, and J. Newman, *J. Electrochem. Soc.*, **147**, 99 (2000).
23. A. Hjelm and G. Lindbergh, *Electrochim. Acta*, **47**, 1747 (2002).
24. T. S. Ong and H. Yang, *J. Electrochem. Soc.*, **149**, A1 (2002).
25. J. S. Hong and J. R. Selman, *J. Electrochem. Soc.*, **147**, 3190 (2000).
26. C. Montella, *J. Electroanal. Chem.*, **518**, 61 (2002).
27. A. V. Churikov and A. V. Ivanischev, *Electrochim. Acta*, **48**, 3677 (2003).
28. H. Shin and S. Pyun, in *Modern Aspects of Electrochemistry*, No. 36, C. G. Vayenas, B. E. Conway, R. E. White, and M. E. Gamboa-Adelco, Editors, Plenum, New York (2003).
29. Q. Wang, H. Li, X. Huang, and L. Chen, *J. Electrochem. Soc.*, **148**, A737 (2001).
30. G. Sikha, B. N. Popov, and R. E. White, *J. Electrochem. Soc.*, **151**, A1104 (2004).
31. P. Ramadass, B. Haran, P. M. Gomadam, R. E. White, and B. N. Popov, *J. Electrochem. Soc.*, **151**, A1196 (2004).
32. B. Barnes and G. R. Fulford, *Mathematical Modeling with Case Studies*, Taylor and Francis, New York (1998).
33. M. Ozisik, *Boundary Value Problems of Heat Conduction*, Dover Publications, New York (1968).
34. S. Devan, V. S. Subramanian, and R. E. White, *J. Electrochem. Soc.*, **152**, A947 (2005).
35. A. Varma, M. Morbidelli, and H. Wu, *Parametric Sensitivity in Chemical Systems*, Cambridge University Press, New York (1999).